Research in Astron. Astrophys. **2009** Vol. **9** No. **5**, 558 – 576
http://www.raa-journal.org *http://www.iop.org/journals/raa*

***R**esearch in*
***A**stronomy and*
***A**strophysics*

Polarization variability arising from clumps in the winds of Wolf-Rayet stars *

Qing-Kang Li[1,3], Joseph P. Cassinelli[2], John C. Brown[3] and Richard Ignace[4]

[1] Department of Astronomy, Beijing Normal University, Beijing 100875, China; *qkli@bnu.edu.cn*
[2] Department of Astronomy, University of Wisconsin-Madison, 53711, USA; *cassinelli@astro.wisc.edu*
[3] Department of Physics and Astronomy, University of Glasgow, Glasgow, G12 8QQ, Scotland, UK; *john@astro.gla.ac.uk*
[4] Department of Physics and Astronomy, Eastern Tennessee State University, USA; *ignace@etsu.edu*

Received 2008 November 18; accepted 2009 March 16

Abstract Polarimetric and photometric variability of Wolf-Rayet (WR) stars as caused by clumps in the winds is revisited. In our model, which is improved from Li et al., radial expansion of the thickness is accounted for, but we retain dependence on the β velocity law and stellar occultation effects. We again search for parameters that can yield results consistent with observations in regards to the mean polarization $\bar{p}$, the ratio $\mathcal{R} = \sigma_{\rm p}/\sigma_{\rm phot}$ of polarimetric to photometric variability and the volume filling factor $f_{\rm V}$. Clump generation and spatial distribution are randomized by the Monte Carlo method so as to produce clumps which are, in the mean, distributed uniformly in space and have time intervals that obey a Gaussian distribution. The generated clumps move radially outward with a velocity law determined by a β index, and the angular size of clumps is assumed to be fixed. By fitting the observed $\sigma_{\rm p}/\sigma_{\rm phot}$ and the volume filling factor $f_{\rm V}$, clump velocity law index β (~ 2) and clump ejection rate $\mathcal{N}$ (~ 1) are inferred, and are found to be well constrained. In addition, the subpeak features of broad emission lines seem to support the clump ejection rate. Meanwhile, the fraction of total mass loss rate that is contained in clumps is obtained by fitting observed polarization. We conclude that this picture of the clumps' properties produces a valuable diagnostic of WR wind structure.

Key words: stars: mass loss — stars: Wolf-Rayet — stars: winds, outflows

1 INTRODUCTION

The intrinsic polarization of hot stars results from the scattering of starlight by electrons in aspherical stellar winds. There is evidence that the asymetry is not from a fixed structure but rather from stochastic ejection of clumps from the base of hot star winds. This evidence has been accumulating from a variety of spectropolarimetric studies which show that variability appears in a wide range of timescales of days, weeks, and months (Lupie & Nordsieck 1987; Taylor et al. 1991). In the case of Wolf-Rayet stars, detailed observational data on the photometric, polarimetric, and spectral line profile variability have been presented and discussed by numerous authors (e.g., St.-Louis et al. 1987; Drissen et al. 1987; Robert et al. 1989; Drissen et al. 1992; Moffat & Robert 1992; Robert 1992; Lepine et al. 2000). Moffat

* Supported by the National Natural Science Foundation of China.

& Robert (1992) and Lepine & Moffat (1999) have interpreted the Wolf-Rayet observations in terms of a distribution of dense clumps which result from hierarchical turbulence in the stellar winds. Brown et al. (1995) have discussed some of the physical properties of the larger clumps which dominate aspects of the data. Brown (1993) and Brown et al. (1999) conclude that clumps arise either by localized mass loss enhancements at the stellar surface or by the action of radiatively driven shocks sweeping up material on large scales. Brown et al. (2004) have discussed the combined effects of clumping and multiple scattering on the "momentum paradox" of WR star winds.

With the systematic monitoring campaigns of WR stars, Robert et al. (1989) and Robert (1992) find that WR stars statistically display polarization of about 0.1%, and show broad band polarimetric variation ($\sigma_{\rm p} \approx 0.1\% - 0.02\%$) that is much smaller than the fractional photometric variability ($\sigma_{\rm phot}$), with the mean ratio being about $\mathcal{R} = \sigma_{\rm p}/\sigma_{\rm phot} \approx 0.05$. Richardson et al. (1996) investigate the statistical effect of having larger numbers of clumps present and conclude that the clumps must be very dense so that their emission ($\propto n^2 V$) is large enough to increase $\sigma_{\rm phot}$ and/or their optical depth is large enough to reduce $\sigma_{\rm p}$ by multiple scattering. Li et al. (2000) revisited the analysis by carrying out numerical simulations, following clump flows from the star with a β velocity law while accounting for the occultation of clumps behind the stellar disk, but while also retaining the single scattering assumption. They concluded that clumps follow a large β velocity index, which means that the clumps are accelerating relatively slowly with respect to radius. They also derived a certain range of clump ejection rate that, along with β, allows for a fit to the statistical data. Valuable constraints on WR parameters, such as mass loss rate, can be inferred from the observed mean polarization $\bar{p}$ (about 0.1% level), the polarimetric and photometric variances. These conclusions are supported when considered in conjunction with the number of distinct narrow features that are seen in emission line profiles.

As for observational evidence of clumping of hot stars in other wavebands, Ignace, Quigley & Cassinelli (2003) used the observations with the Infrared Space Observatory (ISO) SWS spectrometer to constrain the velocity law and wind clumping, and found that a β-value of the velocity law of the wind is about 2 – 3 and the volume filling factor is up to 40% for WR 136. Marchenko et al. (2006) obtain numerous overdense clumps in the wind of WR 135 with FUSE observations. Chandra high resolution spectral observations of line profiles have shown the clumping wind properties of hot stars (Owocki & Cohen 2006; Oskinova, Hamann & Feldmeier 2007; Cassinelli et al. 2008).

Recently, Davies et al. (2007) used the clump-ejection model to study the polarimetric variability of hot stars, in particular, of luminous blue variables (LBVs), and got detailed clump parameters through their simulations. One of their conclusions is that many tiny clumps are ejected around hot stars. Of particular interest to us is that Davies et al. (2007) find a flaw in the assumptions of Li et al. (2000), in their assumption that both the thickness of a clump is fixed and the number of electrons in a clump is constant. These results from Davies et al. (2007) motivate us to update the model of Li et al. (2000). It is our goal to understand the general nature of Wolf-Rayet stars, using a picture for ejection of clumps into the wind. Here, we allow the thickness of a clump to vary with wind flow. We find that the main conclusions in Li et al. (2000) still hold, and that the present model leads to good constraints on the parameters, such as β and $\mathcal{N}$.

The basic model scenario is presented in Section 2, where the basic formulation concerned with polarization and scattering of light from both a single clump and an ensemble of clumps is taken into account for various β and $\mathcal{N}$. In Section 3, the model results are presented and discussed, and in Section 4, general conclusions are presented.

2 CLUMPING MODEL

2.1 Basic Formulation of Polarization for a Single Clump

We assume that the polarimetric and photometric variability of a WR star is due to localized mass ejections at the stellar surface, over which clumps are generated at random positions, and at random time intervals according to a normal distribution with mean value Δt. The clumps are then taken to move radially outward with a velocity law. Thus, the thickness Δr of the clump should simultaneously

expand along radial wind flows, while solid angle $\Delta\Omega$ is assumed constant (the geometry of a single outflowing clump is shown in Fig. 1). The electron density then decreases as $r^{-2}\,v^{-1}(r)$. Clumps thus have axisymmetric shapes and, on the assumption that they are not optically thick in the continuum, the results of Brown & Mclean (1977) can be used to find the polarization of a single clump as:

$$p = \tau_{\rm opt}\,(1-3\gamma)\sin^2 i, \tag{1}$$

where

$$\tau_{\rm opt} = \frac{3}{16}\sigma_{\rm T}\int_{r_1}^{r_2}\int_{\mu_2}^{\mu_1} n(r,\mu)\,dr\,d\mu \tag{2}$$

is a mean optical depth, and

$$\gamma = \frac{\int_{r_1}^{r_2}\int_{\mu_2}^{\mu_1} n(r,\mu)\mu^2\,dr\,d\mu}{\int_{r_1}^{r_2}\int_{\mu_2}^{\mu_1} n(r,\mu)\,dr\,d\mu} \tag{3}$$

is a "shape" factor. i is the clump axis inclination to the line of sight; $\mu = \cos\vartheta$, where ϑ is the clump opening angle between the axis of symmetry and the direction of scatter seen from the center of the star; $n(r,\mu)$ is the electron number density in the clump; and $\sigma_{\rm T}$ is the Thomson scattering cross-section. For the local reference frame (r,ϑ) chosen, we let $\mu_1 = 1$. Given constant solid angle $\Delta\Omega$, electron density is assumed to vary only with distance, i.e., as $n(r,\mu) = n(r)$. To calculate the electron density in one clump, we use the mass conservation law:

$$\dot{M}_b = \Delta\Omega\,r^2\,\rho(r)\,v(r), \tag{4}$$

where $\dot{M}_b$ is mass outflow rate within one clump, $\rho(r)$ is mass density, and $v(r)$ is the radial velocity law that the clump will follow, which we adopt to be of the common form:

$$v(r) = v_\infty\left(1-\frac{b\,R_*}{r}\right)^\beta, \tag{5}$$

where v_∞ is the terminal clump speed, R_* is the photospheric radius of the WR star (We note that there are dynamical and effective optical photospheric notations, see Brown et al. 1995), b is a dimensionless parameter to ensure that initial wind speed is non-zero ($b = 0.995$ is adopted throughout the simulations), and β is a velocity law index, one of our basic clump parameters.

Electron density in a clump thus becomes

$$\begin{aligned} n_e &= \frac{\rho}{\mu_e\,m_{\rm H}} \\ &= \frac{\dot{M}_b}{\mu_e\,m_{\rm H}\,\Delta\Omega\,r^2\,v}, \end{aligned} \tag{6}$$

where $m_{\rm H}$ is hydrogen mass, μ_e is mean particle weight per free electron.

To deal with the finite star geometry, the point source depolarization correction factors $D(r/R_*), C(r/R_*,\chi)$ can be employed according to Cassinelli et al. (1987) and Brown et al. (1989),

$$\begin{aligned} D &= \sqrt{1-\frac{R_*^2}{r^2}} \\ &= \sqrt{1-\frac{1}{x^2}}, \end{aligned} \tag{7}$$

and

$$C = \frac{8 - D(1+D)\,(1-3\cos^2\chi)}{3(1+D)(1+\cos^2\chi)}, \tag{8}$$

where $x = r/R_*$, again R_* is the photospheric radius of the WR star, and χ is the scattering angle.

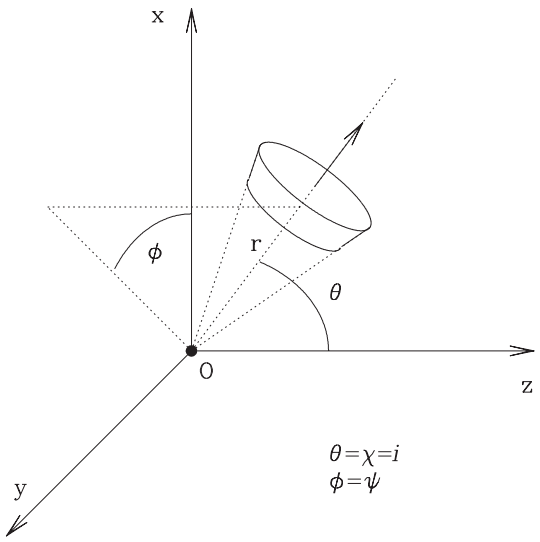

Fig. 1 Geometry of scattering from one clump. We employ a spherical coordinate system (r, θ, ϕ) with oz along the line of sight. For each clump, the "inclination" angle i is identical to the scattering angle χ as well as the polar angle θ, while the polarization position angle in the sky, ψ, is the coordinate component ϕ (see Li et al. 2000).

We wish to combine Equations (1) to (8) to yield an expression for the polarization from a single clump with assumed geometry. After the dimensionless treatment of r (i.e., $r_1/R_* = x_1$ and $r_2/R_* = x_2$), the polarization expression now becomes

$$\begin{aligned} p &= \frac{3}{16}\,\sigma_{\rm T}\,n_o\,R_*\,(1-\mu_2)(\mu_2+\mu_2^2)\sin^2\chi \int_{x_1}^{x_2}\left(\frac{x}{x-b}\right)^{\beta}\frac{D(x)\,dx}{x^2} \\ &= \frac{3}{16}\,\sigma_{\rm T}\,n_o\,R_*\,(1-\mu_2)(\mu_2+\mu_2^2)\sin^2\chi \\ &\quad\times\int_{x_1}^{x_2}\left(\frac{x}{x-b}\right)^{\beta}\frac{1}{x^2}\sqrt{1-\frac{1}{x^2}}\,dx, \end{aligned} \tag{9}$$

and the scattered light intensity $f_{\rm s}$ as a fraction of $L_*/4\pi$ in terms of Brown et al. (1995) is

$$\begin{aligned} f_{\rm s} &= \frac{3}{16}\,\sigma_{\rm T}\,n_o\,R_*\,(1-\mu_2)(1+\cos^2\chi)\int_{x_1}^{x_2}\left(\frac{x}{x-b}\right)^{\beta}\frac{C(r,\chi)\,dx}{x^2} \\ &= \frac{3}{16}\,\sigma_{\rm T}\,n_o\,R_*\,(1-\mu_2) \\ &\quad\times\int_{x_1}^{x_2}\frac{8-D(1+D)(1-3\cos^2\chi)}{3(1+D)x^2}\left(\frac{x}{x-b}\right)^{\beta}dx, \end{aligned} \tag{10}$$

where $n_o = \dot{M}_b/(\mu_e\,m_{\rm H}\,\Delta\Omega\,{R_*}^2\,v_\infty)$.

2.2 Inference of Conservation of Electrons in a Clump

It is assumed that the clump has an initial extent of radial thickness $\Delta x = x_2 - x_1$ ($= 0.01$, for example) and solid angle $\Delta\Omega$ ($= 0.04$, for example), and that the solid angle remains fixed. As the clump moves

radially outward, obeying the velocity law, its thickness will naturally change to expand radially with both the outer face and inner face obeying the local velocity expression. We may explicitly obtain the number of electrons in one clump

$$\begin{aligned} N_e &= \int_0^{2\pi}\int_{\mu_1}^{\mu_2}\int_{r_1}^{r_2} n_e dV \\ &= \frac{\dot{M}_b R_*}{\mu_e\, m_{\rm H}\, v_\infty}\int_{x_1}^{x_2}\frac{dx}{(1-b/x)^\beta}, \end{aligned} \tag{11}$$

where $dV = -r^2\, d\mu\, d\phi dr$ in a local spherical coordinate, and for the geometry of the assumed clump, one may get $\mu_1 = 1$ and $\Delta\Omega = 2\pi(1-\mu_2)$.

In Equation (11), for given values of β and initial Δx, the integral can be solved analytically and/or numerically. In this work, we adopt three acceleration cases: $\beta = 0.5$ for a rapidly accelerating flow; $\beta = 1$, a commonly assumed value for hot star winds; and $\beta = 2$ for the slow acceleration case. These are chosen so that we can determine which case provides an improved fit for WR observational properties.

(1) In case of $\beta = 0.5$, we may analytically do the integral in Equation (11) and obtain

$$\begin{aligned} N_e &= \frac{\dot{M}_b R_*}{\mu_e\, m_{\rm H}\, v_\infty}\int_{x_1=1}^{x_2}\frac{\sqrt{x}}{\sqrt{x-b}}dx \\ &= \frac{\dot{M}_b R_*}{\mu_e\, m_{\rm H}\, v_\infty}\left[\sqrt{x(x-b)} + b\ln\left(\sqrt{x}+\sqrt{x-b}\right) + {\rm con1}\right]_{x_1}^{x_2} \\ &= N_{e0}\left(\sqrt{x_2(x_2-b)} - \sqrt{x_1(x_1-b)} + b\ln\frac{\sqrt{x_2}+\sqrt{x_2-b}}{\sqrt{x_1}+\sqrt{x_1-b}}\right) \\ &= N_{e0}\left[\sqrt{x(x-b)} + b\ln\left(\sqrt{x}+\sqrt{x-b}\right) + {\rm con1}\right]_1^{1+0.01}, \end{aligned} \tag{12}$$

where con1 is a constant from the integral and $N_{e0} = \frac{\dot{M}_b R_*}{\mu_e\, m_{\rm H}\, v_\infty}$ is also a constant for the given stellar parameters. Owing to the boundary condition assumed, i.e. $x_2 = x_1 + \Delta x = 1 + 0.01$ at $x_1 = 1$, the expression $\left[\sqrt{x(x-b)} + b\ln\left(\sqrt{x}+\sqrt{x-b}\right) + {\rm con1}\right]_1^{1+0.01}$ is equal to 0.103. Therefore, Equation (12) can clearly yield the following equation

$$\sqrt{x_2(x_2-b)} - \sqrt{x_1(x_1-b)} + b\ln\frac{\sqrt{x_2}+\sqrt{x_2-b}}{\sqrt{x_1}+\sqrt{x_1-b}} = 0.103. \tag{13}$$

(2) In case of $\beta = 1$, we use the same method above and get the equation

$$x_2 - x_1 + b\ln\frac{x_2-b}{x_1-b} = 1.103. \tag{14}$$

(3) In case of $\beta = 2$, we repeat the same process and obtain the following equation

$$x_2 - x_1 + 2b\ln\frac{x_2-b}{x_1-b} + \frac{b^2(x_2-x_1)}{(x_1-b)(x_2-b)} = 134.2. \tag{15}$$

Equations (13), (14), or (15) set up the coherent relationship between x_1 and x_2. We may use them with a given value of β to get x_2 once x_1 is specified. In these simulations, we use the Newtonian bisection and bracketing methods to solve Equations (13), (14), or (15) due to the nonlinear relationship between x_1 and x_2. Note, it is clearly shown that the number of electrons in a clump with various β values are different ($N_e = N_{e0}\times 0.103$ for $\beta = 0.5$, $N_e = N_{e0}\times 1.103$ for $\beta = 1$ and $N_e = N_{e0}\times 134.2$ for $\beta = 2$). [We may also have a special case of $\beta = 0$, which will give the value of the integral equal to Δx (Δx=0.01) and then we will have the expression $N_e = N_{e0}\times 0.01$ for $\beta = 0$.] The electron scattering in the clump results in polarization, hence the number of electrons will affect the strength of polarization, as discussed in Section 3.

2.3 Relation between Time t since Clump Expulsion and Clump Distance r from the Star

The radial thickness varies with time as the clump moves out. We can connect the time since expulsion of a particular clump with its current radial distance from the velocity law. Similarly, given time t, the clump distance (say r) can be obtained. From the clump velocity law, this relationship is,

$$\begin{aligned} t &= \int \frac{dr}{v(r)} \\ &= \frac{R_*}{v_\infty} \int \frac{dx}{(1-b/x)^\beta} \\ &= \tau \int \frac{dx}{(1-b/x)^\beta}, \end{aligned} \tag{16}$$

where $\tau = R_*/v_\infty$ is denoted as the "flow time scale."

Again, in the case of $\beta = 0.5$,

$$\begin{aligned} \frac{t}{\tau} &= \int \frac{\sqrt{x}}{\sqrt{x-b}} dx \\ &= \sqrt{x(x-b)} - \frac{b}{2} \ln \left[\frac{x-b}{b} \left(\sqrt{\frac{x}{x-b}} - 1 \right)^2 \right] + \mathrm{con2}. \end{aligned} \tag{17}$$

If we adopt $x = 1$ at $t = 0$ and use $b = 0.995$, then we will get $\mathrm{con2} = -0.14$ in Equation (17). Therefore, the expression between time and distance is

$$\frac{t}{\tau} = \sqrt{x(x-b)} - \frac{b}{2} \ln \left[\frac{x-b}{b} \left(\sqrt{\frac{x}{x-b}} - 1 \right)^2 \right] - 0.14. \tag{18}$$

In the cases of $\beta = 1$ and $\beta = 2$, the expression between time and distance are, respectively,

$$\frac{t}{\tau} = x + b \ln(x-b) + 4.27, \tag{19}$$

and

$$\frac{t}{\tau} = x - b + 2b \ln(x-b) - \frac{b^2}{x-b} + 208.55. \tag{20}$$

Therefore, from numerical experiments, t/τ may be accumulated in a stepwise manner by doing summation of $\Delta t/\tau$, and $\Delta t/\tau$ is chosen to have a Gaussian distribution.

2.4 Polarization for an Ensemble of Clumps

The expressions above for polarization and scattering are for a single clump. To account for many clumps, we use the same approach as in Li et al. (2000). We set up a spherical coordinate system (r, θ, ϕ) with the polar axis oz being along the line of sight. Then for each clump, the "inclination" angle i is identical to both the scattering angle χ and the polar angle θ, while the polarization position angle in the sky, ψ, is just the coordinate component ϕ (see Fig. 1).

For a system of clumps labeled $j = 1, N$, the total scattered light fraction f_s and the net polarization are as usual for the optically thin case, simply given by the sum over j the Stokes intensity parameters $Q_j = p_j \cos 2\phi_j$, $U_j = p_j \sin 2\phi_j$ of each to get the totals of Q and U, then finding $p = (Q^2 + U^2)^{1/2}$ and position angle $\Psi = \frac{1}{2} \arctan \frac{U}{Q}$. It is to be understood that *summations exclude all occulted clumps* – i.e. clumps whose coordinates x_j, θ_j, ϕ_j satisfy $\theta_j > \pi/2$ and $x_j \sin \theta_j < 1$. Note that $\mu_j = \cos \theta_j$ is uniformly sampled in the interval -1 to $+1$ and ϕ_j from 0 to 2π . The radii x_j are determined by time and the velocity law.

Total mass loss rate $\dot{M}$ is distributed among all clumps and the ambient, inhomogeneous but, on average, spherical "wind." We choose the fraction of mass loss in clumps to be η. Hence, $\eta\dot{M} = \dot{N}N_e\mu_e m_{\rm H}$, where $\dot{N}$ is the mean clump ejection rate (s^{-1}) and N_e again is the total number of electrons in one clump. Thus, if we fix $\dot{M}$ and increase $\dot{N}$ then there are more clumps in any given range of r but each would have smaller N_e. We denote $\mathcal{N} = \dot{N}\,\tau$, the number of clumps ejected per characteristic flow time ($\tau = R_*/v_\infty$), as the measure of the clump ejection rate. If we assume a portion of the total mass lost is flowing into k clumps and that each has the same number of electrons, then there is a scaling relationship $\eta\dot{M} = k\dot{M}_b$. Since in a flow time τ, there are $\mathcal{N}$ clumps ejected, we can attain $k \sim \mathcal{N}$. Therefore, we may replace $\dot{M}_b$ in Equation (6) with $\eta\dot{M}/\mathcal{N}$ when accounting for many clumps in the simulations.

The system of equations governing the time varying polarization and scattered light is then

$$\begin{aligned} Q &= \sum_{j=1}^{N} Q_j \\ &= \frac{3}{16}\,\sigma_{\rm T}\,n_o\,R_*(1-\mu_2)(\mu_2+\mu_2^2)\sum_{j=1}^{N}\sin^2\theta_j\,\cos 2\phi_j \\ &\quad\times\int_{x_1}^{x_2}\left(\frac{x_j}{x_j-b}\right)^{\beta}\frac{1}{x_j^2}\sqrt{1-\frac{1}{x_j^2}}\,dx_j \\ &= \frac{3}{16}\,\sigma_{\rm T}\frac{n_o'}{\mathcal{N}}R_*(1-\mu_2)(\mu_2+\mu_2^2)\sum_{j=1}^{N}\sin^2\theta_j\,\cos 2\phi_j \\ &\quad\times\int_{x_1}^{x_2}\left(\frac{x_j}{x_j-b}\right)^{\beta}\frac{1}{x_j^2}\sqrt{1-\frac{1}{x_j^2}}\,dx_j \\ &= \frac{p_0}{\mathcal{N}}\sum_{j=1}^{N}\sin^2\theta_j\,\cos 2\phi_j\int_{x_1}^{x_2}\left(\frac{x_j}{x_j-b}\right)^{\beta}\frac{1}{x_j^2}\sqrt{1-\frac{1}{x_j^2}}\,dx_j, \end{aligned} \tag{21}$$

and

$$\begin{aligned} U &= \sum_{j=1}^{N} U_j \\ &= \frac{3}{16}\sigma_{\rm T}\,n_o\,R_*(1-\mu_2)(\mu_2+\mu_2^2)\sum_{j=1}^{N}\sin^2\theta_j\sin 2\phi_j \\ &\quad\times\int_{x_1}^{x_2}\left(\frac{x_j}{x_j-b}\right)^{\beta}\frac{1}{x_j^2}\sqrt{1-\frac{1}{x_j^2}}\,dx_j \\ &= \frac{3}{16}\sigma_{\rm T}\frac{n_o'}{\mathcal{N}}R_*(1-\mu_2)(\mu_2+\mu_2^2)\sum_{j=1}^{N}\sin^2\theta_j\sin 2\phi_j \\ &\quad\times\int_{x_1}^{x_2}\left(\frac{x_j}{x_j-b}\right)^{\beta}\frac{1}{x_j^2}\sqrt{1-\frac{1}{x_j^2}}\,dx_j \\ &= \frac{p_0}{\mathcal{N}}\sum_{j=1}^{N}\sin^2\theta_j\sin 2\phi_j\int_{x_1}^{x_2}\left(\frac{x_j}{x_j-b}\right)^{\beta}\frac{1}{x_j^2}\sqrt{1-\frac{1}{x_j^2}}\,dx_j, \end{aligned} \tag{22}$$

where $n'_o = \eta\dot{M}/(\mu_e\, m_{\rm H}\, \Delta\Omega\, {R_*}^2\, v_\infty)$ and

$$\begin{aligned} p_0 &= \frac{3}{16}\sigma_{\rm T} n'_o R_*(1-\mu_2)(\mu_2+\mu_2^2) \\ &= \frac{3}{16}\sigma_{\rm T}\frac{\eta\dot{M}}{\mu_e\, m_{\rm H}\, \Delta\Omega {R_*}^2 v_\infty} R_*(1-\mu_2)(\mu_2+\mu_2^2). \end{aligned} \tag{23}$$

Hence, the total polarization is given by

$$p = \sqrt{Q^2+U^2}, \tag{24}$$

and

$$\begin{aligned} f_{\rm s} &= \sum_{j=1}^{N} f_{\rm sj} \\ &= \frac{3}{16}\sigma_{\rm T} n_o R_*(1-\mu_2) \\ &\quad \times \sum_{j=1}^{N}\int_{x_1}^{x_2} \frac{8 - D_j(1+D_j)(1-3\cos^2\theta_j)}{3(1+D_j)x_j^2}\left(\frac{x_j}{x_j-b}\right)^{\beta} dx_j \\ &= \frac{3}{16}\sigma_{\rm T}\frac{n'_o}{\mathcal{N}} R_*(1-\mu_2) \\ &\quad \times \sum_{j=1}^{N}\int_{x_1}^{x_2} \frac{8 - D_j(1+D_j)(1-3\cos^2\theta_j)}{3(1+D_j)x_j^2}\left(\frac{x_j}{x_j-b}\right)^{\beta} dx_j \\ &= \frac{f_0}{\mathcal{N}}\sum_{j=1}^{N}\int_{x_1}^{x_2} \frac{8 - D_j(1+D_j)(1-3\cos^2\theta_j)}{3(1+D_j)x_j^2}\left(\frac{x_j}{x_j-b}\right)^{\beta} dx_j, \end{aligned} \tag{25}$$

where

$$\begin{aligned} f_0 &= \frac{3}{16}\sigma_{\rm T} n'_o R_*(1-\mu_2) \\ &= \frac{3}{16}\sigma_{\rm T}\frac{\eta\dot{M}}{\mu_e\, m_{\rm H}\, \Delta\Omega\, {R_*}^2\, v_\infty} R_*(1-\mu_2). \end{aligned} \tag{26}$$

Note again, in the above expressions, both x_1 and x_2 are varying with time, so we need to use Equations (13), (14), or (15) in regards to various β to determine x_2 once x_1 is given. Here, x_1 is obtained from Equations (18), (19), or (20) in case of different β, if time t is known from the numerical experiments.

On inspection of the above equations for polarization and scattered light, we expect that, for given $\dot{M}$, $\Delta\Omega$, initial Δr, and β, results should depend mainly on $\mathcal{N}$. For a fixed mass loss rate and flow time, if the clump generation rate is low, only a few clumps, each of high density, will be present near the star and these dominate the p and $f_{\rm s}$ values, as is shown in Li et al. (2000). However, for high generation rates, many low density clumps near the star will be controlling p and $f_{\rm s}$. So, the same total number of electrons is redistributed in different numbers of clumps, resulting in different statistical means and variances in the polarization and scattered light fraction. For a fixed clump ejection and mass loss rate, the number of clumps in the inner radii near the star has a steady mean value. Therefore, they affect the resulting polarization, scattered intensity and resulting variances, but these values change with $\mathcal{N}$, $\dot{M}$, and β. Their observed values allow inference of the clump emission and flow parameters.

3 MODEL RESULTS AND DISCUSSION

1. As a start, let us calculate the thickness, volume and polarization of a single clump while varying its location, supposing $\sin\chi = 1$ and $\beta = 1$. The results are displayed in Figure 2.

In Figure 2a, the solid line denotes the inner radial boundary (say x_1) and the dotted line denotes the outer radial boundary (say x_2). We see that, as time progresses, x_2 increases faster than x_1, which directly induces an expansion in thickness. In Figure 2a, for comparison, x_2 ($x_2 = x_1 + \Delta x$) with constant thickness $\Delta x = 0.01$ is shown in the dashed line which almost overlaps the solid line x_1. In Figure 2b, the solid line denotes the case for which a constant clump thickness is assumed. In contrast, the dotted line shows the expansion of thickness with its location (i.e. x), and we see that thickness increases rapidly from $x = 1$ to $x = 2$, where winds are mainly accelerated. In Figure 2c, the solid line denotes the volume of the clump with constant thickness $\Delta x = 0.01$ and the dotted line denotes the volume of the clump with expanding thickness, which is increasing dramatically faster than the constant thickness case. We compare the polarization of varying thickness (the dotted line in Fig. 2d) with that in Davies et al. (the solid line in Fig. 2d) for one single clump and see that in both cases, the polarization decreases as the clump moves outward, while there is a peak polarization about $x = 1.2$ for the latter case.

2. Furthermore, we calculate the thickness, volume and polarization of a single clump while varying its location, supposing $\sin\chi = 1$ but with different β, as is shown in Figure 3. To see how x_1 varies

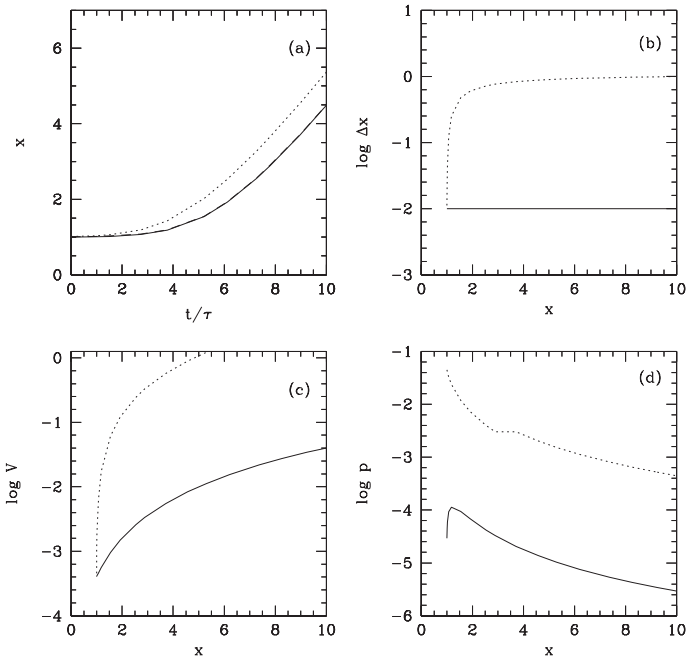

Fig. 2 Model results are shown for a single clump: (a) The radial extent vs. time. The solid line denotes the inner radial boundary (say x_1) and the dotted line denotes the outer radial boundary, x_2 ($x_2 = x_1 + \Delta x$) with a constant thickness $\Delta x = 0.01$, is shown in the dashed line which almost overlaps the solid line x_1. (b) Clump thickness versus clump location. The solid line denotes the constant clump thickness as assumed. In contrast, the dotted line shows the expansion of thickness with its location (i.e. x). (c) Clump volume vs. its location. The solid line denotes the volume of the clump with constant thickness $\Delta x = 0.01$ and the dotted line denotes the volume of the clump with expanding thickness. (d) Polarization vs. clump location. The dotted line is for varying thickness and the solid line is for constant thickness as in Davies et al. (2007).

with time (say t/τ) in case of differing βs, we show the results in Figure 3a in which fast acceleration of $\beta = 0.5$ is displayed by the dashed line and moderate acceleration of $\beta = 1$ is shown in the solid line, and slow acceleration of $\beta = 2$ is given by the dash-dotted line. We also show that the radial thickness varies with location of the clump in Figure 3b. The dash-dotted line denotes the case of $\beta = 2$, the solid line denotes the case of $\beta = 1$, and the dashed line denotes the case of $\beta = 0.5$. In addition, we show the constant thickness case with $\beta = 1$ in the dotted line. In Figure 3c, we show that the volume changes with the clump location in various cases of β as denoted in the figure. In Figure 3d, we show that the polarization varies with location of the clump. The dash-dotted line denotes the case of $\beta = 2$, the solid line denotes the case of $\beta = 1$, and the dashed line denotes the case of $\beta = 0.5$. In addition, we show the constant thickness case in the dotted line. Note that the start values of polarization in various cases of β are different since the electron number in one single clump for various cases of β is different, as is shown from Equation (12) which is related to β. Additionally, polarization is mainly determined by the number of electrons in the clump (Brown et al. 1995).

3. Taking into account the behavior of an ensemble of clumps, we compute the polarization, the fraction of scattering light intensity, and their variations. In particular, we calculate the ratio of their variations for various clump ejection rates $\mathcal{N}$ in a flow time with various $\beta = 0.5$, 1, 2. Interestingly, $\sigma_{\rm p}/\bar{p}$ and $\sigma_{\rm p}/\sigma_{\rm phot}$ do not depend on any specific star, but only on $\mathcal{N}$ and β. This is not surprising since p (or $f_{\rm s}$) linearly relies on p_0 (or f_0) which is determined by the parameters of a star. So, we can treat $\sigma_{\rm p}/\sigma_{\rm phot}$ as a probe to explore the probable $\mathcal{N}$ and β. To get rid of the influence of any specific star,

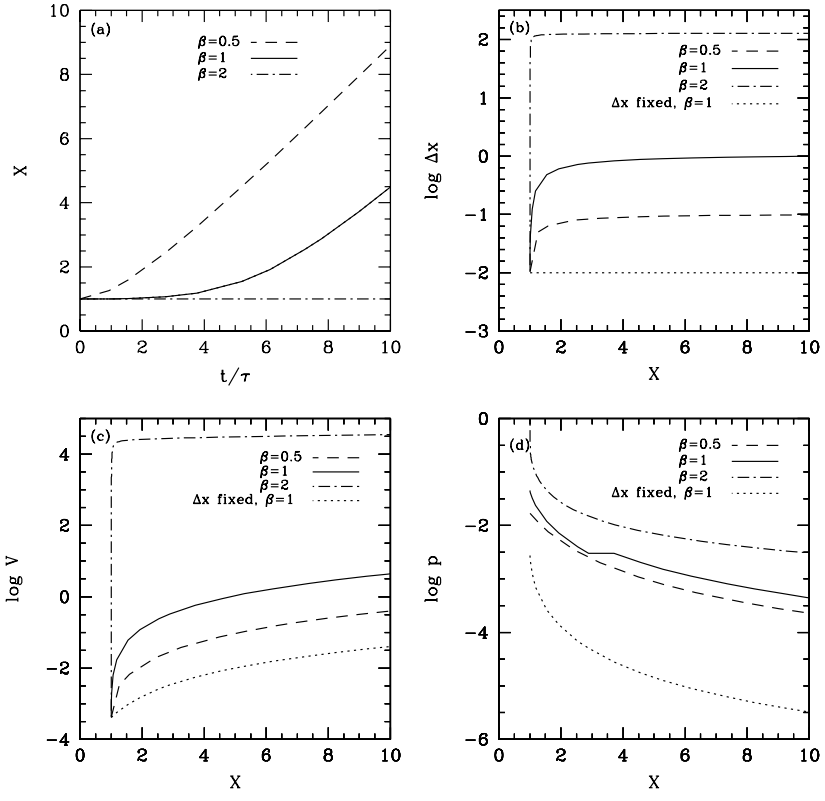

Fig. 3 Model results are displayed in various cases of β as denoted in the figure for one single clump.

we divide p (as well as Q and U) in Equation (24) by p_0 in Equation (23) and divide $f_{\rm s}$ in Equation (25) by f_0 in Equation (26). The results are displayed in Tables 1, 2 and 3. Using the values in these tables, we plot $\sigma_{\rm p}/\bar{p}$ and $\sigma_{\rm p}/\sigma_{\rm phot}$ with various $\mathcal{N}$ in cases of various $\beta = 0.5,\ 1,\ 2$. The observed value of $\sigma_{\rm p}/\bar{p} = 0.5$ is denoted by the dotted line in the upper panel of Figure 4, and the observed value of $\sigma_{\rm p}/\sigma_{\rm phot} = 0.05$ is denoted by the dotted line in the lower panel of Figure 4. We found that to achieve the observed value, three patterns could hold, for $\beta = 0.5 \longrightarrow \mathcal{N} \sim 500$; for $\beta = 1 \longrightarrow \mathcal{N} \sim 150$; and for $\beta = 2 \longrightarrow \mathcal{N} \sim 1$. Although there seems no unique solution for β and $\mathcal{N}$ in terms of the above considerations, while combining the effects of $\mathcal{N}$ and β on $\sigma_{\rm p}/\sigma_{\rm phot}$ and $f_{\rm V}$ the volume filling factor, it seems the observed data might prefer the case of $\mathcal{N} = 1$ and $\beta = 2$. We will further demonstrate this later.

Table 1 Simulation results for a finite star source with occultation and velocity law with $\beta = 0.5$ (total number of clumps applied in the simulations N =5000).

$\mathcal{N}$	$\bar{p}'$	$\sigma'_{\rm p}$	$\bar{f}'_{\rm s}$	$\sigma'_{\rm phot}$	$\bar{p}/\overline{f_{\rm s}}$	$\sigma_{\rm p}/\sigma_{\rm phot}$	$f_{\rm V}$
1/4	0.8394	0.8632	4.928	4.470	0.337	0.382	0.0001
1	0.3565	0.2032	2.319	1.138	0.305	0.353	0.0003
5	0.1557	0.0816	1.927	0.276	0.160	0.479	0.0016
10	0.1091	0.0557	1.891	0.234	0.114	0.473	0.0033
50	0.0500	0.0265	1.835	0.195	0.054	0.271	0.0164
100	0.0364	0.0204	1.783	0.239	0.040	0.168	0.0328
200	0.0268	0.0146	1.693	0.304	0.031	0.094	0.0654
1000	0.0143	0.0051	1.229	0.424	0.023	0.024	0.3190
2000	0.0102	0.0031	0.910	0.392	0.022	0.016	0.6239

Notes: Col. 1 is the clump ejection rate in a flow time. Col. 2 is $\bar{p}' = \bar{p}/p_0$. Col. 3 is $\sigma'_{\rm p} = \sigma_{\rm p}/p_0$. Col. 4 is $\bar{f}'_{\rm s} = \bar{f}_{\rm s}/f_0$. Col. 5 is $\sigma'_{\rm phot} = \sigma_{\rm phot}/f_0$. Col. 6 is $\bar{p}/\bar{f}_{\rm s}$. Col. 7 is $\sigma_{\rm p}/\sigma_{\rm phot}$. Col. 8 is the volume filling factor $f_{\rm V}$.

Table 2 Simulation results for a finite star source with occultation and velocity law with $\beta = 1$ (total number of clumps applied in the simulations N =5000).

$\mathcal{N}$	$\bar{p}'$	$\sigma'_{\rm p}$	$\bar{f}'_{\rm s}$	$\sigma'_{\rm phot}$	$\bar{p}/\overline{f_{\rm s}}$	$\sigma_{\rm p}/\sigma_{\rm phot}$	$f_{\rm V}$
1/4	2.8922	2.1003	22.762	17.995	0.252	0.231	0.0015
1	1.4512	0.7755	15.340	5.933	0.187	0.259	0.0035
5	0.6270	0.3205	14.144	2.371	0.088	0.268	0.0175
10	0.4432	0.2223	14.077	1.753	0.062	0.251	0.0350
50	0.2066	0.1172	13.805	1.664	0.030	0.140	0.1725
80	0.1641	0.0982	13.565	1.985	0.024	0.098	0.2727
100	0.1458	0.0904	13.395	2.170	0.022	0.082	0.3381
150	0.1189	0.0703	13.021	2.557	0.018	0.054	0.4962
200	0.1054	0.0510	12.663	2.852	0.016	0.035	0.6460
400	0.0788	0.0279	11.316	3.529	0.014	0.016	1.1568
1000	0.0506	0.0153	8.065	3.647	0.013	0.008	2.2168
2000	0.0255	0.0088	4.986	2.591	0.010	0.007	4.0601

Notes: Parameters have the same meaning as that in Table 1.

Hamann & Koesterke (1998) found the clump volume filling factor of WR subtype WN stars was about 30% in terms of their spectrum analyses. In this paper, we are able to calculate the clump volume filling factor from our model. The volume filling factor, denoted as $f_{\rm V}$, is defined in common notation as the ratio of the total volume that clumps occupy to the whole volume of space, in which clumps are imbedded

$$f_{\rm V} = \frac{\sum_{i=1}^{N} \Delta V_i}{\frac{4\pi}{3}(r^3 - R_*^3)}. \tag{27}$$

Table 3 Simulation results for a finite star source with occultation and velocity law with $\beta = 2$ (total number of clumps applied in the simulations N =5000).

$\mathcal{N}$	$\bar{p}'$	$\sigma'_{\rm p}$	$\bar{f}'_{\rm s}$	$\sigma'_{\rm phot}$	$\overline{p}/\overline{f_{\rm s}}$	$\sigma_{\rm p}/\sigma_{\rm phot}$	$f_{\rm V}$
1/4	247.339	126.392	17517.453	3157.450	0.028	0.079	0.1071
1	124.8503	64.1338	17300.174	1918.061	0.014	0.066	0.4098
5	48.1358	28.5260	16625.262	2933.660	0.006	0.019	1.7094
10	33.3430	17.1025	15757.138	3900.831	0.004	0.009	2.6139
50	14.3191	3.7360	9381.283	4799.212	0.003	0.002	1.3993
80	9.6549	2.6050	6372.940	3492.983	0.003	0.002	3.3746
100	7.8479	2.1951	5201.766	2891.146	0.003	0.002	5.6845
150	5.2524	1.4971	3550.873	2009.073	0.003	0.002	12.349
200	3.8611	1.0675	2689.970	1536.053	0.003	0.001	11.362
400	1.9001	0.5064	1352.113	778.007	0.003	0.001	15.412
1000	0.7599	0.2026	540.961	311.203	0.008	0.001	15.406
2000	0.3800	0.1013	270.565	155.602	0.003	0.001	15.396

Notes: Parameters have the same meaning as that in Table 1.

We present the model results of $f_{\rm V}$ in Col. 9 of Tables 1, 2 and 3 in case of various βs. We also plot $f_{\rm V}$ vs. $\mathcal{N}$ in Figure 5, in which the dotted line denotes the "observed" value of 30%. The figure shows $\beta = 0.5 \longrightarrow \mathcal{N} \sim 700$; $\beta = 1 \longrightarrow \mathcal{N} \sim 100$; $\beta = 2 \longrightarrow \mathcal{N} \sim 1$, in regards to what is observed. Note, $f_{\rm V}$ greater than 1 means clumps are overlapped or merged. So, for the assumption of thin clumps, we would rule out cases where $f_{\rm V} > 1$.

In general, hot star winds show the property of having two-components: smooth flows and clumps. Of course, when the clumps move farther outward, they will become part of the interstellar medium. However, the density of clumps is, in fact, higher than that of the ambient wind around the star within several hundred stellar radii. The smaller the value of the volume filling factor, the stronger the wind clumping. A clumping wind may cause higher emission for the same amount of material, which implies that the mass loss rates by spectroscopic analysis under the assumption of a smooth wind are systematically overestimated, typically by a factor of $\frac{1}{\sqrt{f_{\rm V}}} \sim 2$ and higher, and the mass loss rates, in turn, consequently affect the stellar structure and evolution. Such clumping presumably arises from the inherent instability of radiation driven winds and would influence the strength of electron scattering wings, change ionization and line ratios, and cause polarization variability and profile variability. In fact, Abbott et al. (1981) have taken the inhomogeneities (i.e. clumps) of the wind into account and got the relationship of mass loss rate, radio flux, and filling factor. Later, in most models, for simplicity, the inter-clump medium is usually treated as void, which leads to the porous scenario (Owocki & Cohen 2006) for OB stars, as the photons are able to leak freely through large separations between clumps. However, our model clearly indicates that the void treatment for WR stars might likely cast some doubts, since the inter-clump medium, which contributes a very large percentage of the total mass, may play a role in hot wind emission, in particular, near the star. The whole inter-clump medium, being a smooth spherical ambient wind, globally contributes nil to the net polarization due to the cancelation effect of polarization.

4. We compute the photometric and polarimetric intensity and their fluctuations in case of various βs. Figures 6, 8 and 10 show how polarization, position angle, and scattered light intensity change with the total number of clumps emitted from the start. Polarization changes are also shown as a locus in the Q – U plane (see Figs. 6, 8 and 10) which, as expected, shows no strong preferred direction, since the mean structure is quasi-spherical. In Figures 7, 9, and 11, we show "observational" time–smoothed results for the variations in mean polarization and scattered light. Standard deviations, σ, of these quantities are also plotted in these figures. The ratio $\mathcal{R}$ versus total number of clumps N as time progresses is plotted in Figure 12, from which we see that in order to obtain the $sustainable$ $\mathcal{R} = 0.05$ as observed, the pattern of $\beta = 2$ and $\mathcal{N} = 1$ is indeed preferred. This seems comparable to the number of subpeaks of the observed broad line. Given the model quantities $R_* = 10R_\odot$ and $v_\infty = 1800\,{\rm km\ s^{-1}}$, flow time τ is about 4000 s. If in one flow time, there is one new clump occurring ($\mathcal{N} \sim 1$), then in 10 flow times,

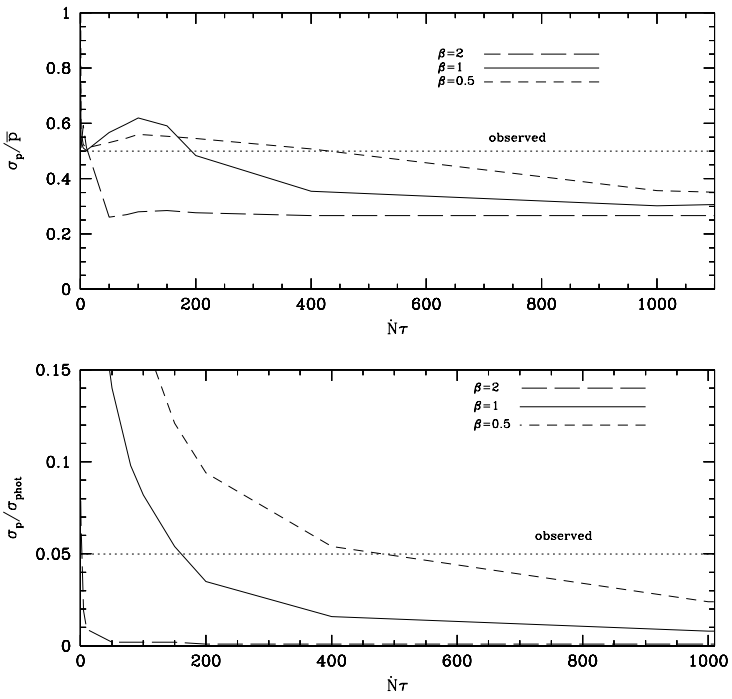

Fig. 4 Upper panel is $\sigma_{\rm p}/\bar{p}$ vs. $\mathcal{N}$ (=$\dot{N}\tau$) in various cases of β as denoted in the plot. The lower panel is $\sigma_{\rm p}/\sigma_{\rm phot}$ vs. $\mathcal{N}$. The observed are denoted as dotted lines in the two panels.

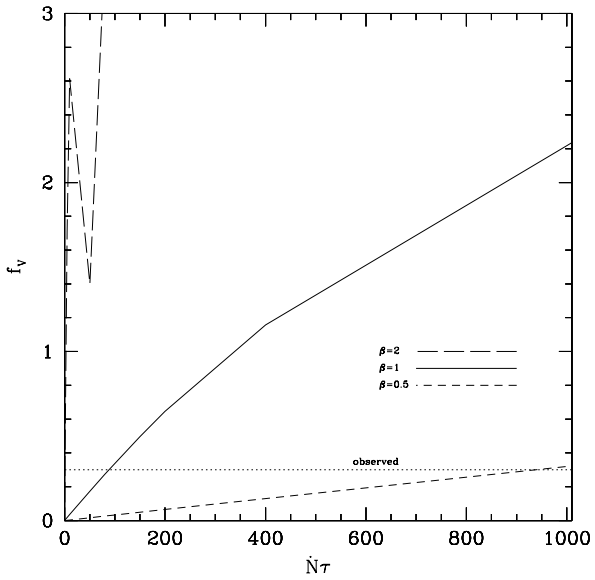

Fig. 5 Volume filling factor $f_{\rm V}$ vs. $\mathcal{N}$ (=$\dot{N}\tau$) in various cases of β as denoted in the plot.

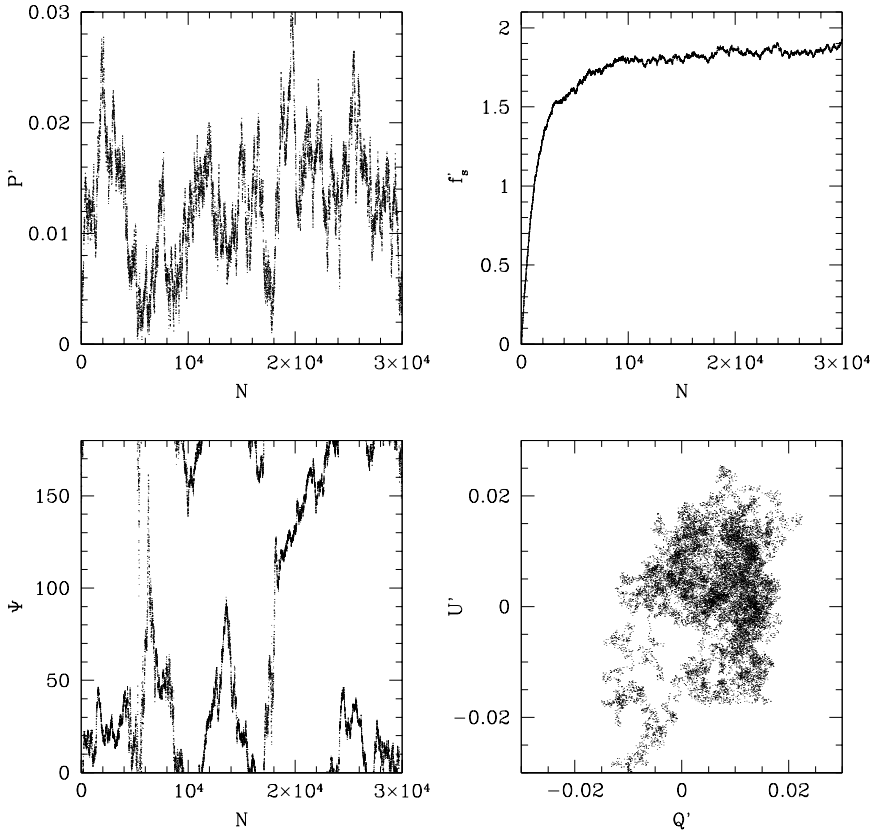

Fig. 6 Figures show respectively, instant by instant, model results vs. number N of clumps emitted thus far for the following: *upper left:* polarization $p' = p/p_0$; *upper right:* scattered light $f_{\rm s}^{'} = f_{\rm s}/f_0$; *lower left:* polarization position angle ψ; *lower right* $Q' = Q(N)/p_0$ vs. $U' = U(N)/p_0$. $\beta = 0.5$ and $\mathcal{N} = 1000$ are applied.

10 new clumps will occur. Hence, there would consequently result in 10 more detectable subpeaks since the clump emission is dominated by the inner clumps in the line emission regions (LERs), which are closer to the star. This conclusion is indeed consistent with observations and their analysis (Robert 1992, Brown et al. 1995). Note, envisaging Tables 1, 2 and 3 in which $\mathcal{R} = 0.05$ seem to be attained, however, observing Figures 6, 8, 10, and their time averaged results in Figures 7, 9, 11, in particular 12, we found that *only* the case of $\beta = 2$ and $\mathcal{N} = 1$ shows a real and sustainable result. Neither the case of $\beta = 1$ and $\mathcal{N} = 200$, nor the case $\beta = 0.5$ and $\mathcal{N} = 1000$, could achieve a long-standing $\mathcal{R} = 0.05$. Therefore, we have to abandon these cases. If we plot the number of clumps versus distance (Fig. 13), we will find that in case of various $\beta = 0.5,\ 1,\ 2$ but with the same $\mathcal{N} = 1$, there will be several hundred clumps radially staggering outward from $1R_*$ to $5R_*$ in case of $\beta = 2$ being very slowly accelerated, but just a few in case of $\beta = 0.5,\ 1$ being rapidly accelerated. In terms of the concept of LER in Lepine & Moffat (1999) and Dessart & Owocki (2005), the LER with velocity space is about 0.4–0.9v_∞ where the clumps are accelerated. We note that the WR-wind acceleration length scale $\beta R_* \sim 20R_\odot$ in their results, is compatible with our results, with $R_* = 10R_\odot$ applied and $\beta = 2$ inferred.

5. For the fraction factor of mass loss rate into clumps η in regards to p_0 in Equation (23) and f_0 in Equation (26), we could use the typical polarization observed for WR stars $\bar{p} = 0.1\% - 1\%$ to constrain

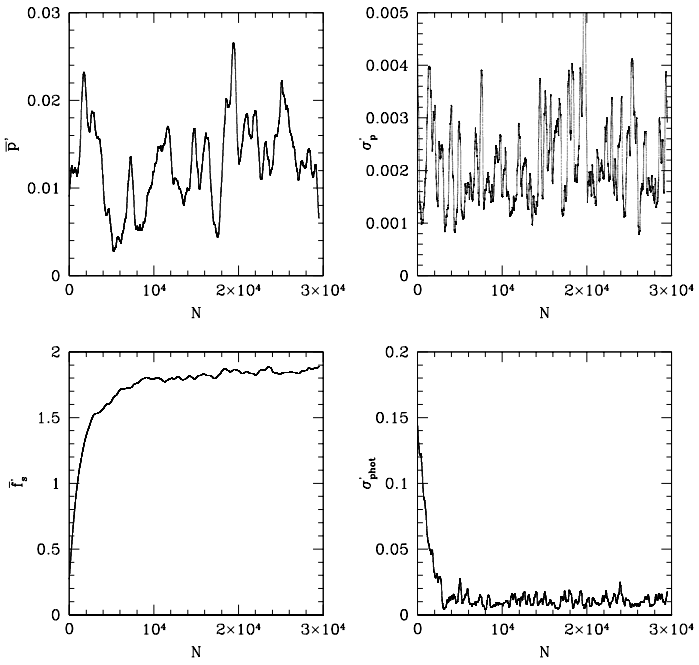

Fig. 7 Based on the same data as Fig. 6, here we show smoothed results versus number of clumps N (increasing with time) for the following observables, with parameters as in Fig. 6. *Upper left:* mean polarization $\bar{p}' = \bar{p}/p_0$; *upper right:* variance of polarization $\sigma_{\rm p}^{'} = \sigma_{\rm p}/p_0$; *lower left:* mean scattered light fraction $\bar{f}_{\rm s}^{'} = \bar{f}_{\rm s}/f_0$; *lower right:* variance of scattered light $\sigma_{\rm phot}^{'} = \sigma_{\rm phot}/f_0$.

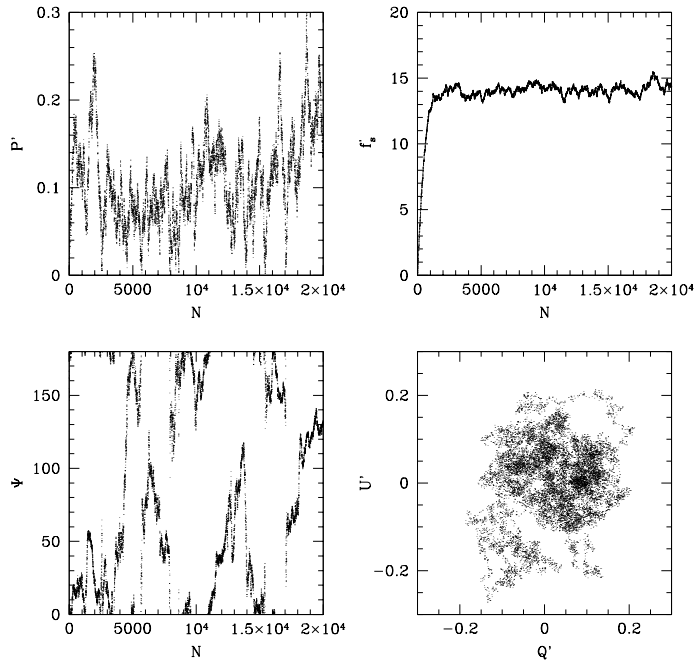

Fig. 8 The figures are similar to Fig. 6, except $\beta = 1$ and $\mathcal{N} = 200$ are applied.

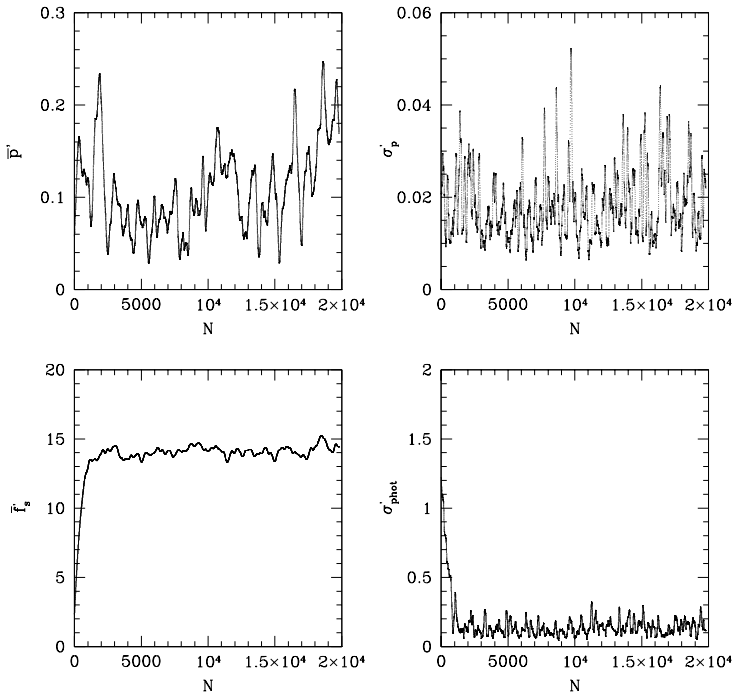

Fig. 9 The figures are similar to Fig. 7, except $\beta = 1$ and $\mathcal{N} = 200$ are applied.

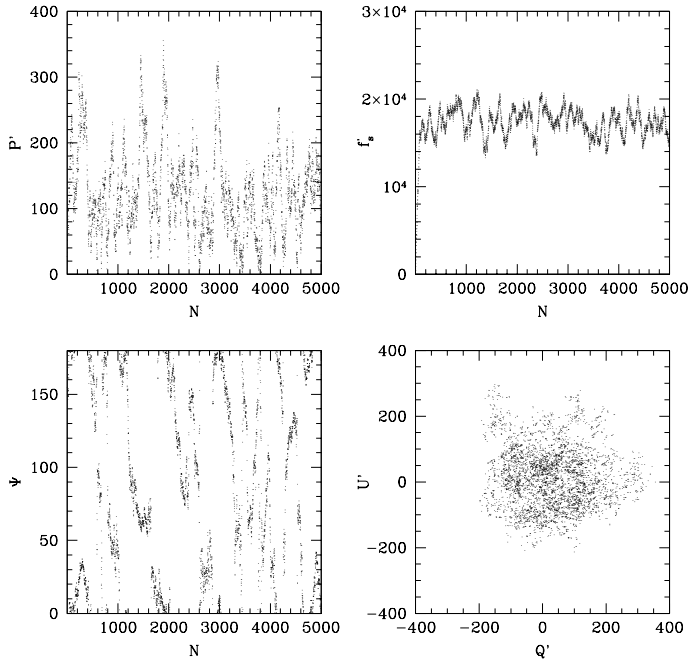

Fig. 10 The figures are similar to Fig. 6, except $\beta = 2$ and $\mathcal{N} = 1$ are applied.

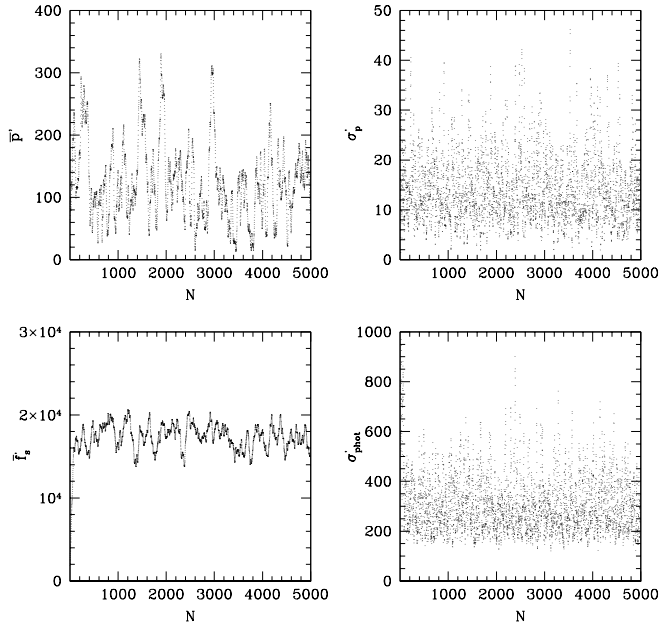

Fig. 11 The resulting figures are similar to Fig. 7, except $\beta = 2$ and $\mathcal{N} = 1$ are applied.

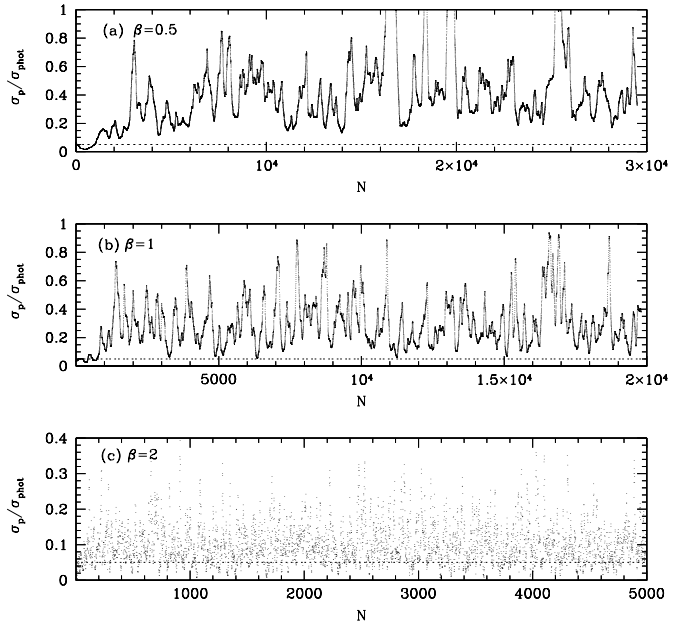

Fig. 12 Ratio ($\mathcal{R} = \sigma_{\rm p}/\sigma_{\rm phot}$) of polarimetric to photometric standard deviations vs. number of clumps N. *Upper panel*: for $\beta = 0.5$ and $\mathcal{N} = 1000$. *Middle panel*: for $\beta = 1$ and $\mathcal{N} = 200$. *Lower panel*: for $\beta = 2$ and $\mathcal{N} = 1$. The steady mean value of $\mathcal{R}$ about 0.05 can be sustainable in case $\beta = 2$ and $\mathcal{N} = 1$.

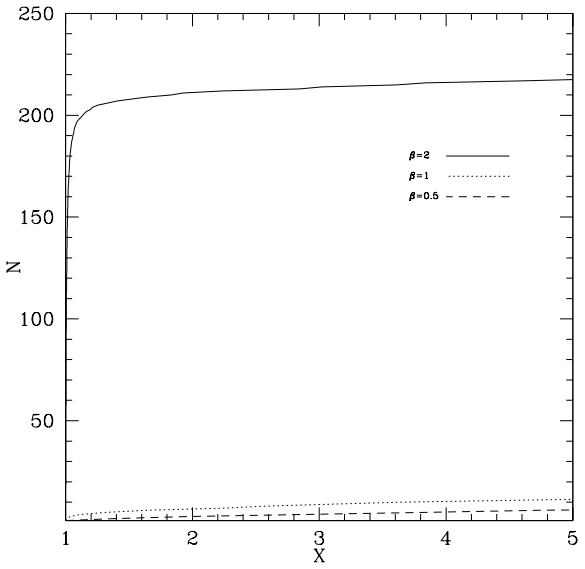

Fig. 13 Number of clumps N vs. radial distance (x) in case $\mathcal{N} = 1$. The solid line is for $\beta = 2$, the dotted line is for $\beta = 1$, and the dashed line is for $\beta = 0.5$. Due to the "dwelling" time around the star being longer in case of larger β, the number of clumps are more, in comparison with the smaller β case.

it. If the following typical parameters are employed: $\dot{M} = 2.5 \times 10^{-6} M_{\odot}$ year^{-1}, $\Delta\Omega = 0.04$, initial $\Delta r_0 = 0.01 R_*$, $\mu_e = 2$, $R_* = 10 R_{\odot}$ and $v_{\infty} = 1800\,\mathrm{km\,s^{-1}}$, then we may gain $p_o = 0.0147\eta$. From the above discussion, the pattern $\beta = 2$ and $\mathcal{N} = 1$ is preferred, then we check Table 3 and get $\bar{p}' = \bar{p}/p_0 \sim 124.85 \longrightarrow \bar{p} = 1.84\eta$. Therefore, we can gain $\eta = \bar{p}/1.84 \sim 10^{-3} - 10^{-2}$. This would imply that only a rather small portion of the winds will deposit mass into the clumps, but most winds are ambient where clumps are embedded. By contrast, one might recall the solar wind picture in which the solar wind is a coherent outward expansion of the solar corona, frequently involving coronal mass ejection (CME) events. Hence, it is not surprising that there are two components in the hot star environments, one being the ambient winds and the other being the clumps (or wind-blown bubbles). However, the formation mechanisms of solar winds and hot star winds are distinctly different. The former is driven by the gas pressure gradient of the high temperature solar corona, and the latter is driven by pressure of radiation emitted by the hot star, the so-called continuum-driven and line-driven. Note that the physical quantities in Tables 1, 2 and 3, such as $\bar{p}' = \bar{p}/p_0$, $\sigma'_{\rm p} = \sigma_{\rm p}/p_0$, $\bar{f}'_{\rm s} = \bar{f}_{\rm s}/f_0$, $\sigma'_{\rm phot} = \sigma_{\rm phot}/f_0$, $\bar{p}/\bar{f}_{\rm s}$, $\sigma_{\rm p}/\sigma_{\rm phot}$, scale with p_0 or f_0, so they are dimensionless numbers. The fraction factor η only affects the values of p_0 and f_0. Thus, for a specific star, one could make a gain in η by incorporating the stellar parameters and observed polarization. We realize that the clumps ejected in our model are massive- or macro-clumps, distinguished from local perturbations in the winds.

4 CONCLUSIONS

In this paper, we update the previous model proposed by Li et al. (2000) and apply the clump ejection scenario to explain WR star wind polarization and its observed variability, by accounting for expansion of clumps along wind flows while keeping the solid angle constant. The main conclusions are as follows.

(1) From numerous model simulations using various β and $\mathcal{N}$, incorporating the volume filling factor $f_{\rm V}$, we found that $\beta \sim 2$ and $\mathcal{N} \sim 1$ are preferred for explaining the observational data of photo-

metric, polarimetric, and spectral line profile variability of WR stars. This gives good model constraints on stellar wind properties of hot stars.

(2) We also found that a small fraction of 10^{-3} of the wind material deposits into clumps but most mass loss goes into space as ambient wind. This quantitative estimation of the mass fraction into the ambient wind implies that porous wind models for WR stars might be used cautiously since the inter-clump medium is far from void.

In summary, this updated model which is improved from Li et al. (2000), with the inclusion of radial expansion of thickness of clumps but retaining dependence on the β velocity law and stellar occultation effects, yields results consistent with observations in regards to mean polarization $\bar{p}$, the ratio $\mathcal{R} = \sigma_{\rm p}/\sigma_{\rm phot}$ of polarimetric to photometric variability, and volume filling factor $f_{\rm V}$. It also offers a quantitative estimation of the mass fraction that goes into clumps and ambient winds. Hence, the model produces a valuable diagnostic of WR wind structure.

Acknowledgements We would like to thank the anonymous referee for constructive comments that led to a significant improvement in the paper. The authors would like to thank Ben Davies for an informative discussion about the work. The authors acknowledge support for this work from: the National Natural Science Foundation of China (grant Nos. 10273002, 10573022 and 10778601 (QL)); the NSF Center for Magnetic Self Organization in Laboratory and Astrophysics Plasmas (JPC); UK STFC Rolling Grant (JCB). JPC and RI have been supported in part by award TM3-4001 issued by the *Chandra* X-ray Observatory Center.

References

Abbott, D. C., Bieging, J. H., & Churchwell, E. 1981, ApJ, 250, 645
Brown, J. C. 1994, Ap&SS 221, 357
Brown, J. C., & McLean, I. S. 1977, A&A, 57, 141
Brown, J. C., Carlaw, V. A., & Cassinelli, J. P. 1989, AJ, 344, 341
Brown, J. C., Ignace, R., & Cassinelli, J. P. 2000, A&A, 356, 619
Brown, J. C., Richardson, L. L., Antokhin, I., Robert, C., Moffat, A. F. J., & St-Louis, N. 1995, A&A, 295,725
Brown, J. C., Richardson, L. L., Ignace, R., & Cassinelli, J. P. 1998, A&A, 330, 253
Brown, J. C., Cassinelli, J. P., Li, Q., Kholtygin, A. F., & Ignace, R. 2004, A&A, 426, 323
Cassinelli, J. P., Nordsieck, K. H., & Murison, M. A. 1987, ApJ, 317, 290
Cassinelli, J. P., Ignace, R., Waldron, W. L., Cho, J., Murphy, N. A., & Lazarian, A. 2008, ApJ, 683, 1052
Davies, B., Vink, J. S., & Oudmaijer, R. D. 2007, A&A, 469, 1045
Dessart, L., & Owocki, S. P. 2005, A&A, 432, 281
Drissen, L., St.-Louie, N., Moffat, A. F. J., & Bastien, P. 1987, ApJ, 322, 888
Drissen, L., Robert, C., & Moffat, A. F. J. 1992, ApJ, 386, 288
Hamann, W. R., & Koesterke, L. 1998, A&A, 335, 1003
Ignace, R., Quigley, M. F., & Cassinelli, J. P. 2003, ApJ, 596, 538
Lepine, S., & Moffat, A. F. J. 1999, ApJ, 514, 909
Lepine, S., Moffat, A. F. J., St-Louis, N., et al. 2000, AJ, 120, 3201
Li, Q., Brown, J. C., Ignace, R., Cassinelli, J. P., & Oskinova, L. M. 2000, A&A, 357, 233
Lupie, O. L., & Nordsieck, K. H. 1987, AJ, 92, 214
Marchenko, S. V., Moffat, A. F. J., St-Louis, N., & Fullerton, A. W. 2006, ApJ, 639, L75
Moffat, A. F. J., & Robert, C. 1992, in ASP Conf. Ser. 22, Nonisotropic and Variable Outflows from Stars, eds. D. Laurent, L. Claus, & N. Antonella (San Francisco: ASP), 203
Oskinova, L. M., Hamann, W.-R., & Feldmeier, A. 2007, A&A, 476, 1331
Owocki, S. P., & Cohen, D. H. 2006, ApJ, 648, 565
Richardson, L. L., Brown, J. C., & Simmons, J. F. L. 1996, A&A, 306, 519
Robert, C. 1992, Ph.D. Thesis, Univ. de Montreal
Robert, C., Moffat, A. F. J., Bastien, P., Drissen, L., & St.-Louie, N. 1989, ApJ, 347, 1034
St.-Louis, N., Drissen, L., Moffat, A. F. J., Bastien, P., & Tapia, S. 1987, ApJ, 322, 870
Taylor, M., Nordsieck, K. H., Schulte-Ladbeck, R. E., & Bjorkman, K. S. 1991, AJ, 102, 1187